Indirubin, the active constituent of a Chinese antileukaemia medicine, inhibits cyclin-dependent kinases

Ralph Hoessel*, Sophie Leclerc†, Jane A. Endicott‡, Martin E. M. Nobel‡, Alison Lawrie‡, Paul Tunnah‡, Maryse Leost†, Eve Damiens†§, Dominique Marie†¶, Doris Marko*, Ellen Niederberger*, Weici Tang*, Gerhard Eisenbrand*# and Laurent Meijer†**

**Department of Chemistry, Division of Food Chemistry and Environmental Toxicology, University of Kaiserslautern, Erwin-Schrödinger-Strasse 52, 67663 Kaiserslautern, Germany*

†Cell Cycle Laboratory CNRS, Station Biologique, BP 74, 29682 Roscoff Cedex, Bretagne, France

¶Phytoplankton Group, CNRS, Station Biologique, BP 74, 29682 Roscoff Cedex, Bretagne, France

‡University of Oxford, Laboratory of Molecular Biophysics, Department of Biochemistry and Oxford Centre for Molecular Sciences, South Parks Road, Oxford OX1 3QU, UK

§Université des Sciences et Technologies de Lille I, Laboratoire de Chimie Biologique, UMR 111 CNRS, 59655 Villeneuve d'Ascq Cedex, France

#e-mail: eisenbra@rhrk.uni-kl.de

***e-mail: meijer@sb-roscoff.fr*

Indirubin is the active ingredient of Danggui Longhui Wan, a mixture of plants that is used in traditional Chinese medicine to treat chronic diseases. Here we identify indirubin and its analogues as potent inhibitors of cyclin-dependent kinases (CDKs). The crystal structure of CDK2 in complex with indirubin derivatives shows that indirubin interacts with the kinase's ATP-binding site through van der Waals interactions and three hydrogen bonds. Indirubin-3′-monoxime inhibits the proliferation of a large range of cells, mainly through arresting the cells in the G2/M phase of the cell cycle. These results have implications for therapeutic optimization of indigoids.

Over four millennia, practitioners of traditional Chinese medicine have accumulated a considerable pharmacopoeia that is largely still used in modern China and in many other parts of the world. The last encyclopaedia of traditional Chinese medicine (1977) lists over 5,500 natural sources (82.8% of which are plants) that form the basis for the 100,000–500,000 prescriptions of traditional Chinese medicine[1,2]. Of these, some are described as relieving 'cancer' (although this term may not always relate to the modern scientific definition of cancer). Several Chinese plants have provided compounds with significant antitumour activity; *Camptotheca acuminata* (camptothecin) and *Cephalotaxus* sp. (homoharringtonine/ harringtonine) are two famous examples[3].

Chronic myelocytic leukaemia (CML) has customarily been treated with the traditional Chinese recipe Danggui Longhui Wan, a mixture of 11 herbal medicines[4]. In 1966, the Institute of Haematology of the Chinese Academy of Medical Sciences embarked on the identification of the active factor of this complex mixture[2–5]. The activity was traced to one ingredient, Qing Dai (indigo naturalis), a dark blue powder prepared from the leaves of *Baphicacanthus cusia* (Acanthaceae), *Polygonum tinctorium* (Polygonaceae), *Isatis indigotica* (Brassicaceae), *Indigofera suffrutticosa* (Fabaceae) and *Indigofera tinctoria* (Fabaceae). This powder contained a high level of the blue dye indigo, but the antileukaemic activity was attributed to the red-coloured isomer of indigo, indirubin, a minor constituent of the mixture[6–11]. Indigo (also known as indigotin) and indirubin (isoindigotin or indigo red) are both derived, by oxidation and dimerization, from indoxyl and isatin, which are themselves liberated from colourless precursor conjugates, indican (from *Indigofera* and *Polygonum* species amongst others) or isatan B (from *Isatis tinctoria*) (refs 12,13 and see Supplementary Information).

Indirubin inhibits DNA synthesis in several cell lines[7,14], in a cell-free assay[15] and *in vivo* in rats with Walker-256 sarcoma[16]. A weak binding of indirubin to DNA *in vitro* has been described[17]. Alterations are seen in the surface morphology of white blood cells and in endoplasmic-reticulum, chromatin and nuclear-envelope structures of peripheral blood samples and bone-marrow leukocytes of patients treated with indirubin[18]. Results of animal studies showed that indirubin exhibits limited toxicity; no effects of indirubin on bone marrow and the production of haematopoietic stem cells have

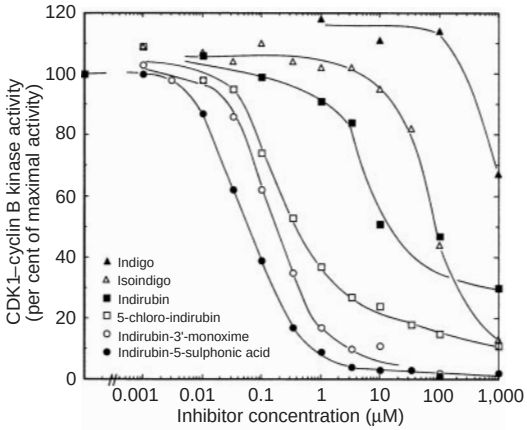

Figure 1 **Inhibition of CDK1–cyclin B by various indigoids.** CDK1–cyclin-B kinase activity towards histone H1 was assayed in the presence of 15 μM ATP and increasing concentrations of indigoids. Activity is presented as a percentage of maximal activity (in the absence of inhibitors).

been observed, even in long-term studies[19–21]. Indirubin shows poor solubility and absorption, so several analogues have been designed in an effort to improve these characteristics[22]. Of these, 5-halogeno-indirubin[23], *N*-ethyl-indirubin[22] and *N*-methylisoindigo[24] exhibited a higher antitumour activity than did indirubin in animal models[23]. Indirubin-3′-monoxime was as active as indirubin in several tumour models[25].

Synthetic indirubin[26] exhibited good antitumour activity and only minor toxicity in animal models[19]. In dogs given a dose of synthetic indirubin 25 times that used for human therapy (according to body weight) continuously for 6 months, diarrhoea and some damage to the liver were observed, with no change in haematopoiesis, electroencephalogram activity and renal functions[27]. In further animal studies, no suppression of haematopoietic stem-cell production by synthetic indirubin was observed[28]. Indirubin has been approved for clinical trials against chronic myelocytic and chronic granulocytic leukaemia (refs 29–32; for reviews see refs 3,27,33). In these studies, 26% of the 314 CML patients showed complete remission and 33% showed partial remission in response to indirubin treatment. Toxicity was low and side effects were limited to mild abdominal pain, diarrhoea, nausea and vomiting. There were three cases of reversible pulmonary arterial hypertension and cardiac insufficiency[34]. A comparative clinical study of CML patients showed that indirubin and busulfan exhibited similar effi-

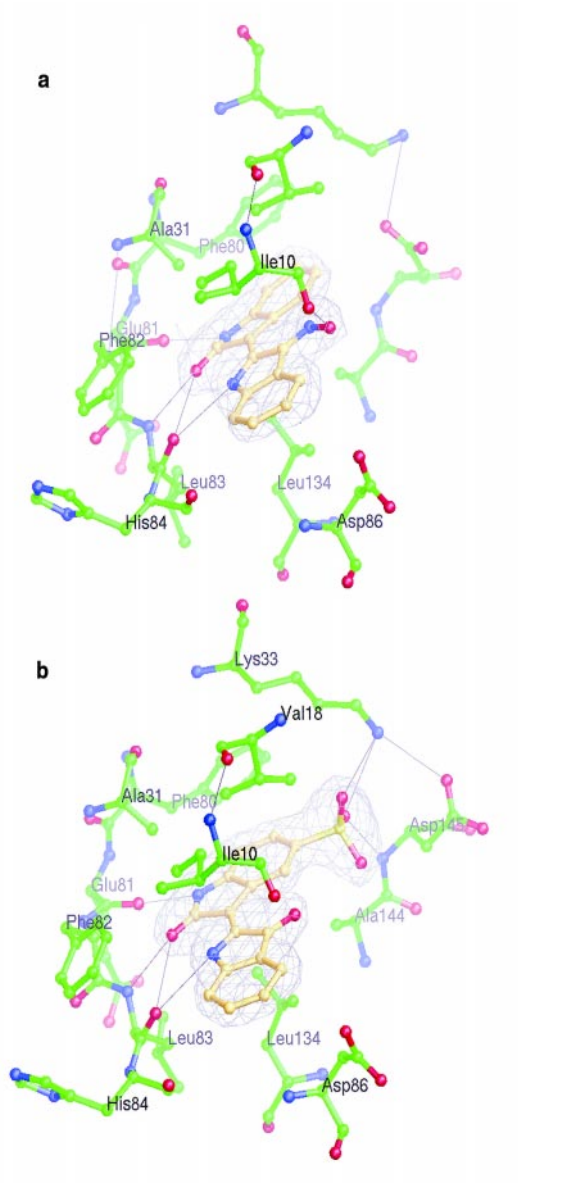

Figure 2 **Binding of indirubin-3′-monoxime and indirubin-5-sulphonate to CDK2. a**, Binding of indirubin-3′-monoxime. **b**, Binding of indirubin-5-sulphonate. CDK2 residues are shown in green, and the indirubin derivatives are shown in yellow. CDK2 residues that contact the bound ligands, as calculated by the CCP4 program Contact[48], are included. Clear electron density defined the residues that interact with the inhibitor molecule. Hydrogen bonds are drawn between the indirubin derivatives and the backbone oxygen of Glu81 of CDK2, and between the indirubin derivatives and the backbone oxygen and nitrogen of Leu83. The figure also includes $(2F_o–F_c)_{\alpha calc}$ electron density for indirubin-3′-monoxime and indirubin-5-sulphonate calculated at the end of refinement using map coefficient output from REFMAC, with resolution between 20 and 2.0 Å. The maps are contoured at a level of **a**, 0.19 e$^-$Å^{-3} and **b**, 0.20 e$^-$ Å^{-3}, corresponding in each case to 1.0 times the root-mean-square deviation of the maps from their mean values.

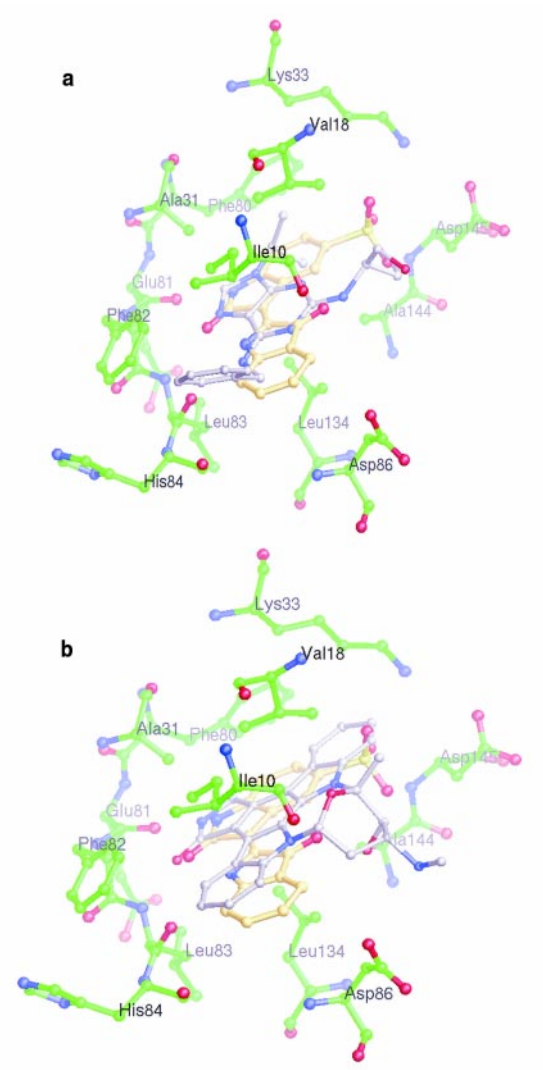

Figure 3 **Superposition of roscovitine and indirubin-5-sulphonate and staurosporine and indirubin-5-sulphonate bound to CDK2. a**, Superposition of roscovitine and indirubin-5-sulphonate bound to CDK2. Indirubin-5-sulphonate is shown in yellow, roscovitine in white and CDK2 in green. **b**, Superposition of staurosporine and indirubin-5-sulphonate bound to CDK2. Colouring as in **a**, with staurosporine in white. The CDK2 residues that contact indirubin-5-sulphonate, as calculated by the CCP4 program Contact, are included. Roscovitine[40] and staurosporine[42] are shown as positioned after superimposing the respective protein structures on the CDK2–indirubin-5-sulphonate complex.

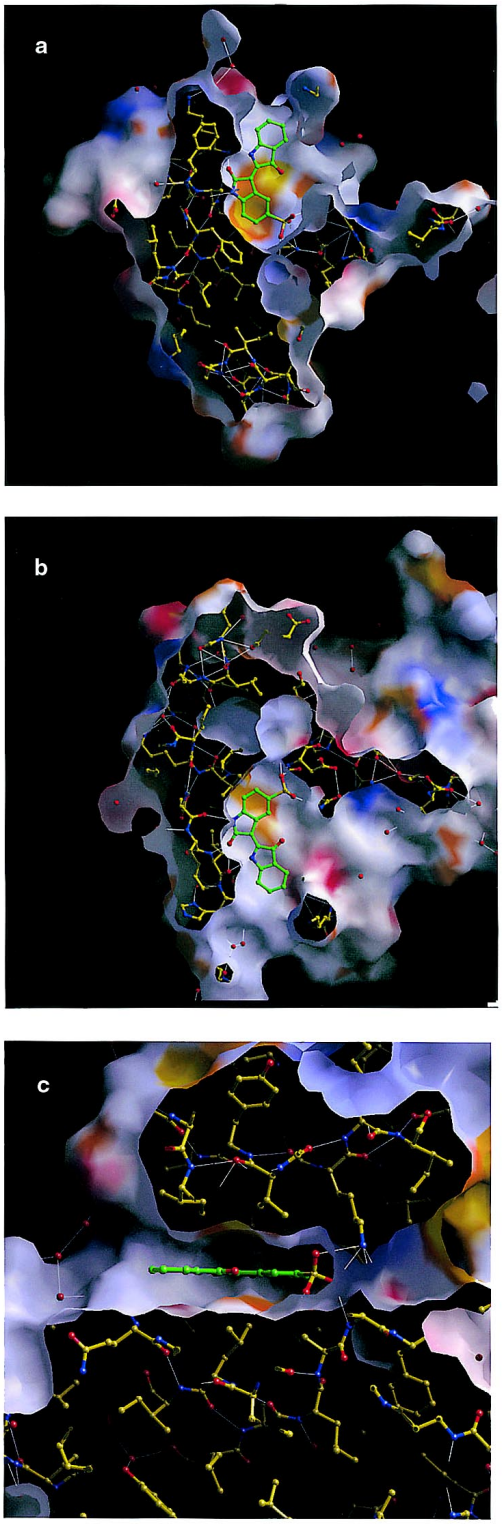

Figure 4 **The Connolly molecular surface of CDK2–indirubin-5-sulphonate, calculated with a probe radius of 1.5 Å.** The surface is coloured by electrostatic potential; blue represents a potential of +15 kT and red a potential of –15 kT. Superimposed on this colour scheme is colouring of hydrophobic potential; regions showing marked hydrophobicity are in yellow. **a**, View looking from the C-terminal domain of CDK2 onto the N-terminal domain. **b**, View from the N-terminal domain onto the C-terminal domain. **c**, Side view, with the CDK2 N-terminal domain above. See Supplementary Information. Ball-and-stick diagrams represent atoms of the CDK2 structure seen through the surface representation.

ciency, with a higher rate of complete remissions observed with busulfan[32]. No crossresistance between the two drugs was observed.

CDKs are crucial in initiating and coordinating the phases of the cell-division cycle[35]. The search for chemical inhibitors of CDKs is mainly inspired by the prospect of identification of new antitumour agents, but such inhibitors may also have applications in other areas, such as psoriasis, cardiovascular diseases, glomerulonephritis, parasitism, viral infections and neurodegenerative disorders[36].

Here, while searching for antineoplastic agents from plants used in traditional Chinese medicine[2], we discovered that indirubin and its analogues selectively inhibit CDKs and block cell proliferation in the late-G1 and G2/M phases of the cell cycle. The crystal structures of CDK2 in complex with two indirubin derivatives reveal the atomic interactions of these inhibitors with the kinase's ATP-binding pocket. It remains to be determined how this molecular effect of indigoids contributes to their antileukaemic properties. Nevertheless, knowledge of this mechanism of action may allow optimization of indigoids as therapeutic antiproliferative agents.

Results

Indirubin and analogues selectively inhibit CDKs. We purified the starfish CDK1–cyclin B complex by affinity chromatography on $p9^{CKShs1}$–Sepharose and assayed its kinase activity towards the substrate histone H1 in the presence of a final ATP concentration of 15 μM, as described[37]. While screening a collection of natural products derived from traditional Chinese medicinal plants[2], we noticed that indirubin exhibited some inhibitory activity towards CDK1–cyclin B (half-maximal inhibitory concentration (IC_{50}) 10 μM) (Fig. 1). In this assay, indigo and isatin were nearly inactive (IC_{50} >1,000 μM and 900 μM, respectively) and isoindigo was only slightly active (IC_{50} 80 μM). Three previously described indirubin derivatives inhibited CDK1 efficiently, namely indirubin-3′-monoxime (IC_{50} 0.18 μM), 5-chloro-indirubin (IC_{50} 0.4 μM) and indirubin-5-sulphonic acid (IC_{50} 0.055 μM) (Fig. 1). These IC_{50} values are comparable to those of previously described CDK inhibitors[36], namely olomoucine (7 μM), roscovitine (0.45 μM), purvalanol (0.004 μM), flavopiridol (0.400 μM), staurosporine (0.006 μM) and butyrolactone (0.600 μM).

We next studied the kinase selectivity of these indigoids. We expressed and/or purified various kinases and assayed them with appropriate substrates as described[37] in the presence of 15 μM ATP and increasing concentrations of indigoids. Table 1 shows IC_{50} values. Most of the 25 kinases tested were not inhibited by indirubin, 5-chloro-indirubin and indirubin-5-sulphonic acid; the inhibitory activities of these indigoids were limited to CDKs. Indirubin, like flavopiridol, inhibited all CDKs equally, but other indigoids showed a preference for CDK1, CDK2 and CDK5 over CDK4. The 3′-monoxime substitution led to a slight reduction in selectivity.

Structures of complexes of CDK2 and indirubin derivatives. To understand the mechanism of action of indigoids better, we co-crystallized two of them with CDK2. The structures of the CDK–indigoid complexes were refined to yield the crystallographic statistics given in Table 2. The structure of CDK2 represents the minimal catalytic kinase core, composed of two domains: a smaller, amino-terminal domain (of ~80 residues) formed mainly from β-sheets, and a larger, predominantly α-helical, carboxy-terminal domain (of ~210 residues). As described previously for both the apo-enzyme and other monomeric CDK2–inhibitor-complex structures[38–43], two regions of CDK2 are flexible in the CDK2–indirubin complex structures. The residues missing from the crystal structure (because they belong to these flexible regions) constitute the loop connecting strand β3 to helix αC (residues 36–43) and the 'activation segment', which contains Thr 160, a residue that is phosphorylated in the fully active CDK2–cyclin-A complex[44] (Table 2). The electron density in the initial F_o–F_c maps showed that the indirubin derivatives bind CDK2 at the ATP-binding site. Fig. 2 shows the electron density for both indirubin derivatives in

Table 1 IC_{50} values for kinase inhibition by indirubin and analogues

Enzyme	Indigo	Indirubin	5-chloro-indirubin	Indirubin-3′-mono-xime	Indirubin-5-sulphonic acid
CDK1–cyclin B	>1,000	10	0.4	0.18	0.055
CDK2–cyclin A	70	2.2	0.75	0.44	0.035
CDK2–cyclin E	>1,000	7.5	0.55	0.250	0.15
CDK4–cyclin D1	>100	12	6.5	3.33	0.3
CDK5–p35	>100	5.5	0.8	0.1	0.065
Erk1	>100	>100	>100	>100	38
Erk2	>100	43	>100	>100	>100
c-Raf	>100	>10	>10	>100	5.5
MAPKK	>100	>100	>100	>100	3
c-Jun N-terminal kinase	>100	>100	21	NT	5.2
Protein kinase C α	>100	>100	>100	27	>100
Protein kinase C β1	>100	>100	>100	4	>100
Protein kinase C β2	>100	>100	>100	20	6.5
Protein kinase C γ	>100	>100	>100	8.4	>100
Protein kinase C δ	>100	>100	>100	>100	>100
Protein kinase C ε	>100	>100	>100	20	>100
Protein kinase C η	>100	>100	>100	52	>100
Protein kinase C ζ	>1,000	>100	>100	>100	>100
cAMP-dependent protein kinase	>1,000	>1,000	600	6.3	>1,000
cGMP-dependent protein kinase	900	>1,000	380	9	480
Casein kinase 1	>100	8.5	28	9	10
Casein kinase 2	>100	>100	>100	12	1.5
Insulin-receptor tyrosine kinase	>1,000	>1,000	550	11	320
c-Src tyrosine kinase	28	18	10	NT	3.8
c-Abl tyrosine kinase	>1,000	>1,000	>1,000	NT	>1,000

Enzyme activities were assayed as described in Methods, in the presence of increasing concentrations of the indigoids indicated. IC_{50} values were calculated from the dose–response curves and are presented in μM. NT, not tested.

final $2F_o–F_c$ maps.

Indirubin-3′-monoxime and indirubin-5-sulphonic acid share a similar binding mode: the lactam amide nitrogen of the inhibitor donates a hydrogen bond to the peptide oxygen of Glu81 of CDK2; the NH group of Leu83 of CDK2 donates a hydrogen bond to the lactam amide oxygen; and the cyclic nitrogen acts as a hydrogen-bond donor to the backbone oxygen of Leu83 (Fig. 2). In comparison with previously reported CDK2–inhibitor structures[38–43], the indirubin derivatives form an extra hydrogen bond with the CDK2 backbone. Like isopentenyladenine, staurosporine (Fig. 3b) and

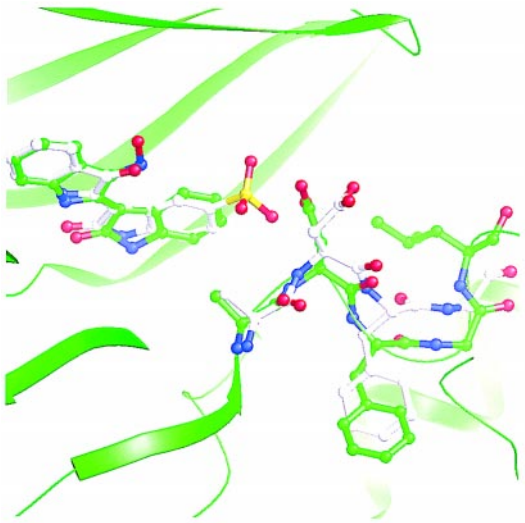

Figure 5 **Movement of the conserved DFG loop accompanies indirubin-5-sulphonate binding to CDK2.** The structures of CDK2–indirubin-3′-monoxime (green) and CDK2–indirubin-5-sulphonate (white) are superimposed; the ligands and residues Asp145, Phe146 and Gly147 are shown here. The site is located within the overall CDK2 model, represented as a ribbon fold. As a result of steric and charge repulsion between the side chain of Asp145 and the sulphonate group of indirubin-5-sulfonate, the DFG loop is rearranged into a conformation that differs from that observed in both the CDK2–indirubin-3′-monoxime and CDK2–ATP structures.

ATP, the indirubin derivatives form hydrogen bonds with the backbone oxygen of Glu 81 and the NH group of Leu83, but the indirubin derivatives also resemble olomoucine or roscovitine in that they also interact with the backbone oxygen of Leu83 (Fig. 3a). Although residues 80–84 of CDK2 constitute part of the hinge between the N- and C-terminal domains, the interactions with indirubin derivatives do not result in a significant change in relative domain orientation. The shape of the indirubin molecule complements the bent shape of the ATP-binding site in the hinge region. This shape complementarity is also observed in the CDK2–staurosporine and CDK2–roscovitine structures (Fig. 3). Indirubin-3′-monoxime and indirubin-5-sulphonic acid make several apolar contacts with conserved residues that line CDK2's ATP-binding site (Fig. 4). Both derivatives contact Phe80 and fill the back of the cleft more completely than either ATP or staurosporine (Fig. 3b). This extra interaction site is also exploited by roscovitine: the N9 isopropyl group packs against the sidechain of Phe80 (Fig. 3a)[40].

The sulphonate group of indirubin-5-sulphonate occupies a site similar to that occupied by one of the rings of staurosporine's extended indole ring system, as seen in the structure of staurosporine bound to CDK2 (ref. 42). The ring systems of these two bound inhibitors are not co-planar. Through its ability to make both charge and hydrogen-bond interactions, the sulphonate group is more complementary to the CDK2 structure in this region than is the staurosporine ring. A superposition of the structures of cyclic-AMP-dependent protein kinase (cAPK)[45], the phosphorylated CDK2–cyclin-A complex[44], the CDK2–ATP complex[43] and the CDK2–indirubin-5-sulphonate complex shows that the sulphonate group does not precisely mimic one of the ATP phosphate groups, as occurs in the other CDK2 structures. However, the sulphonate group of indirubin-5-sulphonate and the α-phosphate of ATP in the cAPK–Mg-ATP–PKI (where PKI is cAMP-dependent protein-kinase inhibitor) ternary complex[45] interact with the sidechain amino group of Lys 33. In addition to this interaction, the sulphonate oxygens contact the backbone nitrogen of Asp 145 and the

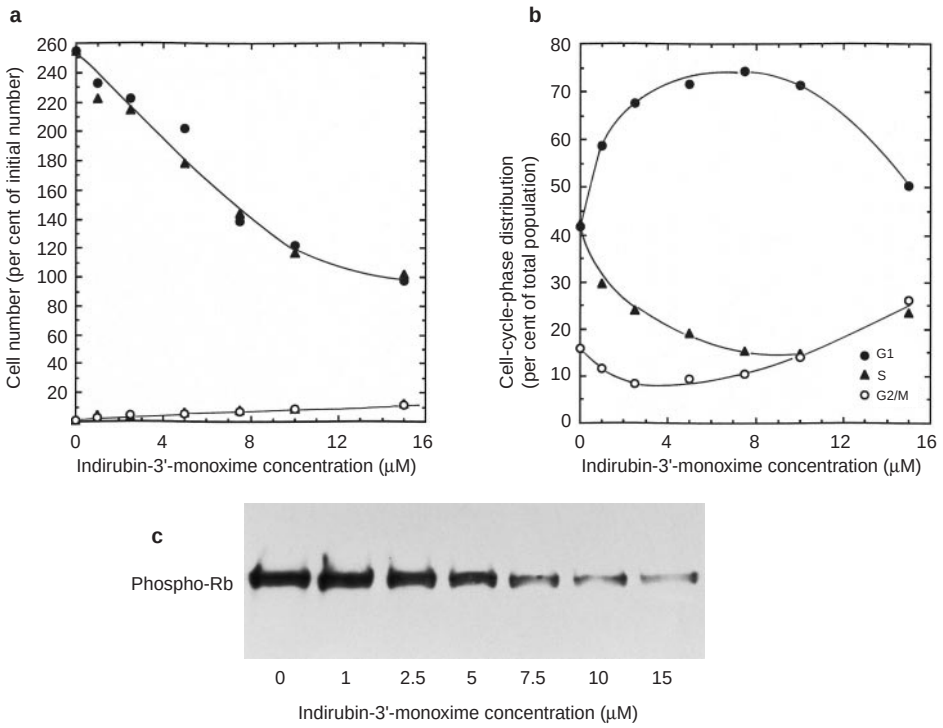

Figure 6 **Indirubin-3′-monoxime inhibits proliferation of Jurkat cells, accumulates cells in G1 and G2/M and reduces phosphorylation of the retinoblastoma protein. a,** Cells were treated for 30 h with various concentrations of indirubin-3′-monoxime and counted. Cell counts (from two independent experiments) are expressed as a percentage of the number of cells at time 0. Filled symbols, living cells; open symbols, apoptotic cells. **b,** Cell-cycle distribution of similarly treated cells, as a function of indirubin-3′-monoxime concentration. **c,** Western blot of total cell extracts with anti-phospho-retinoblastoma-protein antibodies following treatment with increasing concentrations of indirubin-3′-monoxime.

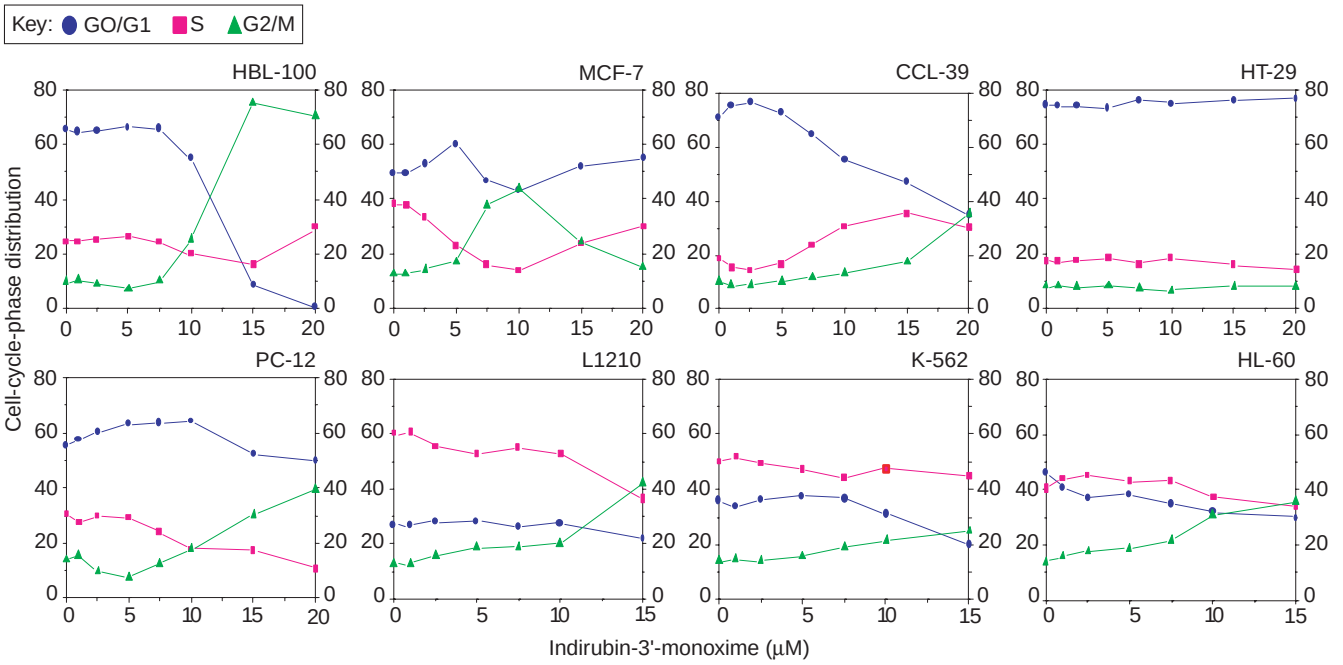

Figure 7 **Cell-cycle-phase distribution of various cell lines following exposure to indirubin-3′-monoxime.** Cells were treated for 30 h with various concentrations of indirubin-3′-monoxime and analysed by FACS (results shown are representative of three independent experiments for each cell line). Note the range in responses, from the most sensitive cell line, HBL-100, to the insensitive HT-29 line. Values on the *y*-axis show percentages of the total cell population.

Table 2 Statistics of the datasets used and of the refined structures

	CDK2–indirubin-3′-monoxime	CDK2–indirubin-5-sulphonic acid
Data collected (space group $P2_12_12_1$)		
Cell dimensions (Å)	53.2, 71.4, 71.6	53.2, 69.5, 71.6
Maximal resolution (Å)	2.20	1.90
Observations	42,821	38,756
Unique reflections (per cent completeness)	13,463 (93.4%)	19,244 (85.9%)
R_{merge}*	0.078	0.045
Mean $I/\sigma(I)$	12.0	17.2
Highest resolution bin (Å)	2.30–2.20	1.99–1.90
Completeness (%)	90.5%	90.4%
mean I/mean σ (I)	2.36	1.66
R_{merge}	0.409	0.403
Refinement statistics		
Protein atoms	2,246	2,217
Residues	1–35, 44–151, 163–298	1–35, 44–147, 163–298
Other atoms	155 water 21 indirubin-3'-monoxime	108 water 24 indirubin-5-sulphonic acid
Resolution range (Å)	20.00–2.20	20.00–1.90
R_{conv}†	0.20	0.22
R_{free}‡	0.30	0.285
Mean protein temperature factors (Å)^2	43.2	47.55
Mean ligand temperature factors (Å)^2	47.7	44.1

* *where:*

$$R_{merge} = \frac{\sum_h \sum_j I_{h,j} - \bar{I}_h}{\sum_h \sum_j I_{h,j}}$$

where $I_{h,j}$ is the intensity of the jth observation of unique reflection h.

† $$R_{conv} = \frac{\sum_h \left| |Fo_h| - |Fc_h| \right|}{\sum_h |Fo_h|}$$

where Fo_h and Fc_h are the observed and calculated structure-factor amplitudes for reflection h.

‡ R_{free} is equivalent to R_{conv}, but is calculated using a 5% disjointed set of reflections excluded from the least-squares refinement stages.

amide group of Asn 132. The Asp 145 side chain is displaced from its position in the CDK2–ATP structure and interacts with the amide group of Asn 132.

Binding of staurosporine to CDK2 causes changes to the main-chain conformation of residues Asp 145, Phe 146, Gly 147 and Leu 148 (Asp 145, Phe 146 and Gly 147 constitute the conserved 'DFG' motif found in most protein kinases). Movement of the DFG motif is required to avoid an unfavourable contact between Asp 145 and staurosporine. This change tends towards that seen in the active form of CDK2 bound to cyclin A[44]. Binding of indirubin-5-sulphonate to CDK2 causes a similar movement of the main chain at residues Asp 145 and Phe 146 as a result of unfavourable steric and charge effects between the sulphonate group and Asp 145 (Fig. 5). Gly 147 can be located in the CDK2–indirubin-5-sulphonate complex electron-density maps, but the following residues that lead into the activation loop cannot be defined and the model resumes at Val 163. In contrast, the CDK2–indirubin-3′-monoxime structure is similar to the CDK2–ATP structure and shows a loop region that is ordered through to residue Ala 151 (Fig. 5). The monoxime group of indirubin-3′-monoxime occupies the ATP-ribose-binding site and makes no direct interactions with CDK2.

Indirubin-3′-monoxime inhibits cell proliferation. We next investigated the effects of various indigoids on cell proliferation. The most potent indigoid, indirubin-5-sulphonic acid, as judged by our *in vitro* kinase assay, had limited effects on cell proliferation, probably because of its limited permeability. We therefore used indirubin-3′-monoxime to study the effects of indigoids on the T-lymphoblastic Jurkat cell line. Indirubin-3′-monoxime inhibited the proliferation of Jurkat cells in a concentration-dependent manner (Fig. 6a). This arrest was associated with a modest increase in the apoptosis rate (see Methods; Fig. 6a). Analysis of the cell-cycle distribution showed a marked G1-phase arrest at low indirubin-3′-monoxime concentrations, whereas at higher concentrations cells accumulated in G2/M phase (Fig. 6b). The G1 arrest was accompanied by a decrease in phosphorylation of the retinoblastoma protein (Fig. 6c). We attribute this effect to inhibition of CDK2 rather than of CDK4–cyclin D (see Table 1), but it could also be an indirect effect (for example, induction of cellular CDK inhibitors such as those induced by DNA damage, or downregulation of cyclin D, whose induction probably involves several protein kinases).

To determine whether the mechanism of growth inhibition of the Jurkat cells was general or dependent on the cell phenotype, we analysed the cell-cycle distribution of various haematopoietic and non-haematopoietic cells following exposure to a range of indirubin-3′-monoxime concentrations. Proliferation of most cell lines was inhibited by indirubin-3′-monoxime in a concentration-dependent manner (Fig. 7). Only the human adenocarcinoma cell line HT-29-18-C1 remained insensitive. Fluorescence-activated cell sorting (FACS) analysis of the cell-cycle distribution showed that indirubin-3′-monoxime, at concentrations over 10 μM, induced arrest at G2/M phase in all the sensitive cell lines analysed. We observed, for the most sensitive cells, another cell-cycle block at lower indirubin-3′-monoxime concentrations (5–10 μM); this block depended on the cell phenotype. For example, MCF-7 and Jurkat cells were arrested at G1 phase and CCL-39 cells were arrested at S phase. These *in vitro* studies confirm and extend our knowledge of the antiproliferative properties of indirubin-3′-monoxime.

Discussion

We have shown that indirubin and its derivatives are potent inhibitors of CDKs. They act by competing with ATP for binding to the catalytic subunit of the kinase. In the future, structural modifications of the indirubin backbone may reveal structure–activity relationships of indigoids (G. E. *et al.*, manuscript in preparation). It will also be interesting to study natural indigoids, which could be obtained by fermentation of indigo-producing plants, of which there are several hundred species in a wide range of distant families. Muricidae and Thaididae molluscs could also provide new and original indigoids to complement the structure–activity study.

The co-crystallization of indigoids with CDK2 reveals many details about the atomic interactions of the inhibitors with the CDK, and will be helpful in the synthesis of new, and hopefully potent, inhibitor analogues. The monoxime derivative may provide a reactive group that can be extended to exploit potential interactions with both the CDK2 glycine-rich loop and the ATP-ribose-binding site. The backbone oxygen of Ile 10 of CDK2 is the closest atom to this reactive group. However, considerable structural rearrangement of the N-terminal domain with respect to the C-terminal domain accompanies binding of CDK2 to cyclin A[43] and there are subtle differences in the glycine-loop conformations

observed in different CDK2–inhibitor complexes. The inherent flexibility of the CDK2 structure in this region may confound attempts to predict other interactions to increase potency or selectivity, and we will probably need to know how the inhibitor binds to the active phosphorylated CDK2–cyclin-A complex. A crystal or structure obtained with an active CDK–cyclin complex, rather than with monomeric CDK2, would be more useful in predicting better inhibitors.

The most potent of the indirubin derivatives, indirubin-5-sulphonate, achieves its potency in part through an ionic interaction with Lys 33 of CDK2. The range of interactions in this region is dependent on restructuring of the DFG loop and reorientation of Lys 33 to a conformation more similar to that observed in the CDK2–cyclin-A complex. The interaction between the 5-sulphonate group and the conserved lysine is not, however, favourable in all environments: the IC_{50} value for indirubin-5-sulphonate with Erk2 as a substrate is more than a thousandfold higher than that of indirubin.

The orientations of indirubin-3′-monoxime and indirubin-5-sulphonate when bound to CDK2 are nearly identical, indicating that the effects of substitutions at the monoxime and sulphonate positions may be additive. As both classes of substituent give rise to marked increases in potency compared with indirubin, this offers a promising lead in inhibitor development.

Might indirubin's antileukaemic effects be attributable to other properties, rather than an effect on CDK2 activity as suggested here? Indirubin and its derivatives also bind to DNA[17], but structure–activity studies with a series of substituted indirubin derivatives tested in a mouse leukaemia model have shown that the potency of indirubin-monoxime *O*-methyl ether is significantly reduced by addition of a methyl group to the amide nitrogen[25]. This modification is unlikely to interfere with DNA intercalation, but would affect indirubin's ability to bind to CDK2: our structural study shows that such a methyl group would disrupt the hydrogen bond to the backbone oxygen of Glu 81, an essential part of indirubin binding to CDK2. This result supports the proposal that the antileukaemic activity of the indigoids derives in part from their ability to inhibit protein kinases. *N*-methyl-isoindigo (meisoindigo), a substituted isoindigo that differs structurally from indirubin (Fig. 1), has been shown to inhibit microtubule polymerization[24]. However, although we observed a modest inhibition of *in vitro* tubulin polymerization by 20 μM indirubin, indirubin-3′-monoxime had no significant effect, even at concentrations of up to 30 μM, on either *in vitro* polymerization or depolymerization of tubulin (data not shown). Furthermore, isoindigo inhibits DNA synthesis and leads to the accumulation of L1210 cells in S phase[24], an effect not observed with indirubin-3′-monoxime in L1210 cells (Fig. 7).

Our results show that indirubin-3′-monoxime has antiproliferative activity, leading to a G2/M arrest in almost all cell types studied and to G1/S arrest in Jurkat cells, the most sensitive cell line. This latter arrest is associated with an inhibition of phosphorylation of the retinoblastoma protein. These observations are compatible with an *in vivo* inhibition of CDKs. Alternatively, indigoids may act on other proteins. We are now trying to identify cellular targets of indigoids by using affinity-chromatography techniques; this method should allow us to establish the importance of inhibition of CDKs and interaction with other proteins in the antileukaemic properties of indigoids. □

Methods

Chemistry.

Indigo (at least of reagent grade) and isatin (p.A. grade) were obtained from Fluka and used without further purification. Other solvents and reagents were at least of reagent grade. Elemental analyses were performed using a Perkin–Elmer 2400 CHN elemental analyser. [^{1}H]-NMR spectra were recorded at 400 MHz and [^{13}C]-NMR spectra at 100 MHz on a Bruker AMX 400, using tetramethylsilane as an internal standard. Mass spectra were taken in the positive-ion mode under electron impact (70 eV) using a Finnigan MAT 90. The synthesis methods and characterization of indirubin and analogues are available as Supplementary Information.

Reagents and buffers.

Antibodies against the retinoblastoma protein (Ser 807/811 phospho-Rb) were obtained from New England Biolabs and used at a 1:1,000 dilution. The compositions of homogenization buffer, buffer C, bead buffer and Tris buffer saline Tween-20 (TBST) are described in ref. 37. PBS contained 140 mM NaCl, 2.7 mM KCl, 1.5 mM KH_2PO_4 and 8.1 mM Na_2HPO_4, pH 7.2–7.4.

Kinase preparations and assays.

Kinase activities were assayed in buffer C, at 30 °C, at a final ATP concentration of 15 μM. Blank values were subtracted and activities calculated as pmoles of phosphate incorporated per 10-min incubation. Controls were done with appropriate dilutions of dimethyl sulphoxide (DMSO). In a few cases, phosphorylation of the substrate was assessed by autoradiography after SDS–PAGE.

CDK1–cyclin B was extracted in homogenization buffer from M-phase starfish (*Marthasterias glacialis*) oocytes and purified by affinity chromatography on p9CKShs1–Sepharose beads, from which it was eluted by free $p9^{CKShs1}$ as described[37]. The kinase activity was assayed with 1 mg ml^{-1} histone H1 (Sigma type III-S), in the presence of 15 μM [γ-^{32}P]ATP (3,000 Ci mmol^{-1}; 1 mCi ml^{-1}) in a final volume of 30 μl. After a 10-min incubation at 30 °C, 25-μl aliquots of supernatant were spotted onto 2.5 × 3 cm pieces of Whatman P81 phosphocellulose paper, and, 20 s later, the filters were washed five times (for at least 5 min each time) in a solution of 10 ml phosphoric acid per litre water. The wet filters were counted in the presence of 1 ml ACS (Amersham) scintillation fluid. The kinase activity was expressed as a percentage of maximal activity.

CDK2–cyclin A, CDK2–cyclin E, CDK4–cyclin D1, CDK5–p35, His-tagged Erk1 and Erk2, protein kinase C isoforms, the catalytic subunit of cAPK, cGMP-dependent protein kinase, casein kinases 1 and 2, the insulin-receptor tyrosine-kinase domain (CIRK-41), c-Raf, MAP kinase kinase, c-Jun N-terminal kinase (obtained from Promega), c-Src kinase and v-Abl kinase were assayed as described[37].

Expression, purification and crystallization of human CDK2.

Human CDK2 was expressed in Sf9 insect cells using a recombinant baculovirus encoding CDK2 and purified following slight modifications to a published method[46]. Monomeric unphosphorylated CDK2 crystals were grown as described[46].

Data collection and processing.

The CDK2–indirubin-3′-monoxime data set was collected from a crystal soaked for 48 h in 2 mM indirubin-3′-monoxime in 1× mother liquor solution (50 mM ammonium acetate, 10% PEG 3350, 15 mM NaCl and 100 mM HEPES, pH 7.4) plus 20% DMSO. The CDK2–indirubin-5-sulphonate soak conditions were 45 h in 2.5 mM indirubin-5-sulphonate in 1× mother liquor solution plus 5% DMSO. Data for the CDK2–indirubin-3′-monoxime complex was collected on beamline XRAY DIFFRACTION at Elettra, Trieste, and the data set for the CDK2–indirubin-5-sulphonate complex was collected on beamline ID14-3 at the ESRF. In each case, data were collected at 100K after crystals had been transferred briefly to cryoprotectant (mother liquor containing 20% glycerol). Images were integrated with the DENZO package and subsequently scaled and merged using SCALEPACK[47]. Statistics of the data sets used are given in Table 2.

Structure solution and refinement.

The starting model for the structure solution and refinement of both CDK–indirubin complexes was the structure of CDK2 in complex with a small molecule inhibitor refined at 1.4 Å resolution (M.E.M.N., A.L., P.T., J.A.E., unpublished results). Following rigid body refinement of the CDK2 structure, $(F_o-F_c)_{\alpha calc}$ maps included easily interpretable electron density for the bound inhibitors. Indirubin-3′-monoxime or indirubin-5-sulphonate was built into the electron-density map and included in subsequent refinement steps. The indirubin-5-sulphonate structure was built in SYBYL with reference to the small-molecule crystal structure of indirubin. The indirubin-3′-monoxime structure was taken from the Cambridge Structural Database. The model was then refined with alternating cycles of interactive model building and maximum-likelihood refinement using the program REFMAC. Towards the end of the refinement, water molecules were added using ARP. Statistics of the final models are given in Table 2 (see Supplementary Information).

Proliferation, cell-cycle and apoptosis analysis.

The human haematopoietic cell lines Jurkat (lymphoblastic T; from ECACC), K-562 (erythroleukaemic; ATCC) and HL-60 (promyelocytic; ATCC) and the lymphocytic mouse leukaemia L1210 line were grown in RPMI 1640 medium (Gibco BRL) containing 10% FCS, 2 mM L-glutamine and gentamycin (Gibco BRL) at 37 °C, 5% CO_2. The human breast cancer epithelial cell line MCF-7, the SV40-transformed human breast epithelial cell line HBL-100, the hamster fibroblastic cell line CCL-39 (ATCC) and colon adenocarcinoma HT-29-18-C1 cells were cultured in Dulbecco's modified Eagle's medium (DMEM; Gibco) supplemented with 10% FCS, 2 mM L-glutamine and gentamycin at 37 °C, 5% CO_2 (10% CO_2 for the HT-29-18-C1 cells). The rat pheochromocytoma cell line PC12 (ATCC) was grown in DMEM supplemented with 10% FCS, 5% horse serum (Gibco BRL), penicillin (100 units ml^{-1}), streptomycin (100 μg ml^{-1}; Gibco BRL) and Fungizone (0.25 μg ml^{-1}; Gibco BRL).

Exponentially growing Jurkat cells at a cell density of 3×10^5 cells ml^{-1} were seeded into 25-cm^2 flasks (Falcon) and treated for 30 h with complete medium containing 0–15 μM indirubin-3′-monoxime. Cell proliferation was then estimated by direct counting with a haemocytometer and cell viability was assessed by trypan-blue exclusion. In parallel, cell samples were collected by centrifugation and fixed in cold 70% ethanol for 4 h. Fixed cells were washed with PBS and incubated with 5 μg RNase A per ml (Sigma) and stained with 25 μg ml^{-1} propidium iodine (Aldrich) for 30 min at 37 °C. The stained cells were analysed on a Becton Dickinson FACScan cytofluorimeter using the cell FIT Software program (Becton Dickinson immunocytometry system). To analyse the extent of apoptosis and necrosis, cells were seeded at 3×10^5 cells ml^{-1} in a 12-well plate (Nunc) and maintained for 30 h with 0–15 μM indirubin-3′-monoxime. Cells were then stained with propidium iodine and annexin V conjugated with fluorescein isothiocyanate (FITC; Immunotech kit). Briefly, cells were collected by centrifugation and resuspended in cold binding buffer. Annexin-V–FITC and 25 μg propidium iodine ml^{-1} were added to the cell suspension for 10 min at 20 °C in the dark. Data were monitored on the cytofluorimeter with light-scatter channels set on a linear gain and fluorescence channels set on a logarithmic scale. Cells were gated for forward- and side-angle light scatters, and 5,000 fluorescent particles of the gated population were analysed.

For the treatment of other cell lines with indirubin-3′-monoxime, adherent cells at a density of

1×10^5 cells per 500 µl and exponentially growing haematopoietic cells at a density of 2×10^5 cells ml^{-1} were maintained in a 24-well plate (Nunc). Cultures were incubated in complete medium in the presence of indirubin-3′-monoxime at concentrations ranging from 0 to 20 µM for 30 h. Following the 30-h incubation, cells were collected as described for the Jurkat cells and analysed for cell-cycle distribution on a FACSort cytofluorimeter (Becton Dickinson). Cell-cycle analyses were done using MultiCYCLE (P. Rabinowitch). This program models DNA histograms following the algorithm of Dean and Jett as the sum of two gaussian peaks for G1 and G2 cells and of a polynomial function broadened by gaussian variability for S cells. Initially, the fractions of cells in G1 (position of G1 peak, variation coefficient of G1 peak) are estimated interactively and then fitted nonlinearly using the Marquardt alagorithm.

Electrophoresis and western blotting.

For preparation of cell extracts, Jurkat cells treated for 30 h with various concentrations of indirubin-3′-monoxime were pelleted, frozen in liquid nitrogen, and stored at −80 °C. Cell pellets (10^6 cells) were extracted directly with 2× Laemmli sample buffer. Equal amounts of cell lysate proteins were run on 10% SDS–polyacrylamide gels. Western blots were performed as described[37].

RECEIVED 8 FEBRUARY 1999; REVISED 27 MARCH 1999; ACCEPTED 29 MARCH 1999; PUBLISHED MAY 1999.

1. Zhu, Y.-P. & Woerdenbag, H. J. Traditional Chinese herbal medicine. *Pharm. World Sci.* **17,** 103–112 (1995).
2. Tang, W. & Eisenbrand, G. *Chinese Drugs of Plant Origin: Chemistry, Pharmacology, and Use in Traditional and Modern Medicine* (Springer, Heidelberg, 1992).
3. Han, R. Highlight on the studies of anticancer drugs derived from plants in China. *Stem Cells* **12,** 53–63 (1994).
4. *Chinese Pharmacopoeia* Vol. 1 (People's Health Publisher, Beijing, 1995).
5. Institute of Haematology, Chinese Academy of Medical Sciences. Clinical studies of Dang Gui Lu Hui Wan in the treatment of CML. *Chinese J. Intern. Med.* **15,** 86–88 (1979).
6. Wu, L. M., Yang, Y. P. & Zhu, Z. H. Studies on the active principles of indigofera tinctoria in the treatment of CML. *Comm. Chinese Herb. Med.* **9,** 6–8 (1979).
7. Wu, G. Y., Fang, F. D., Liu, J. Z., Chang, A. & Ho, Y. H. Studies on the mechanism of action of indirubin in the treatment of chronic granulocytic leukemia. I. Effects on nucleic acid and protein synthesis in human leukemic cells. *Chinese Med. J.* **60,** 451–454 (1980).
8. Zheng, Q. T., Lu, D. J. & Yang, S. L. Pharmacological studies of indirubin. I. Antitumor effect. *Comm. Chinese Herb. Med.* **10,** 35–39 (1979).
9. Zheng, Q. T., Qi, S. B. & Cheng, Z. Y. Pharmacological studies of indirubin. II. Absorption, distribution and excretion of ^{3}H-indirubin. *Comm. Chinese Herb. Med.* **10,** 19–21 (1979).
10. Zhang, S. X. Studies on the chemical constituents of *Isatis indigotica root. Chinese Trad. Herb. Drugs* **14,** 247–248 (1983).
11. Chen, D. H. & Xie, J. X. Chemical constituents of traditional Chinese medicine Qing Dai. *Chinese Trad. Herb. Drugs* **15,** 6–8 (1984).
12. Hurry, J. B. *The Woad Plant and its Dye* (Oxford Univ. Press, Oxford, 1930).
13. Balfour-Paul, J. *Indigo* (British Mus. Press, London, 1998).
14. Chang, H. M. & But, P. P. H. *Pharmacology and Applications of Chinese Materia Medica* Vol. 2 (ed. Teaneck, N.J.) (World Scientific Pub. Co., Singapore, 1987).
15. Zhang, L., Wu, G. Y. & Qiu, C. C. Effect of indirubin on DNA synthesis *in vitro*. *Acta Acad. Med. Sin.* **7,** 112–116 (1985).
16. Du, D. J. & Ceng, Q. T. Effect of indirubin on the incorporation of isotope labeled precursors into nucleic acid and protein of tumor tissues. *Chinese Trad. Herb Drugs* **12,** 406–409 (1981).
17. Wu, G. Y., Liu, J. Z., Fang, F. D. & Zuo, J. Studies on the mechanism of indirubin action in the treatment of chronic granulocytic leukemia. V. Binding between indirubin and DNA and identification of the type of binding. *Sci. Sin.* **25,** 1071–1079 (1982).
18. Lee, K. *et al.* Ultrastructural study on the mechanism of the therapeutic effect of indirubin for human chronic granulocytic leukemia. *Natl Med. J. China* **59,** 129–132 (1979).
19. Ji, X. J., Zhang, F. R., Lei, J. L. & Xu, Y. T. Studies on the antineoplastic effect and toxicity of synthetic indirubin. *Acta Pharma. Sin.* **16,** 146–148 (1981).
20. Wang, J. H., You, Y. C., Mi, J. X. & Ying, H. G. Effect of indirubin on hematopoietic cell production. *Acta Pharmacol. Sin.* **2,** 241–244 (1981).
21. Sichuan Institute of Traditional Chinese Medicine. Subacute toxicity of indirubin in dogs. *Chinese Trad. Herb Drugs* **12,** 27–29 (1981).
22. Ji, X. J. & Zhang, F. R. Antineoplastic effect of indirubin derivatives and their structure-activity relationship. *Acta Pharm. Sin.* **20,** 137–139 (1985).
23. Gu, Y. C., Li, G. L., Yang, Y. P., Fu, J. P. & Li, C. Z. Synthesis of some halogenated indirubin derivatives. *Acta Pharm. Sin.* **24,** 629–632 (1989).
24. Ji, X. J., Liu, X. M., Li, K., Chen, R. H. & Wang, L. G. Pharmacological studies of meisoindigo: absorption and mechanism of action. *Biomed. Environm. Sci.* **4,** 332–337 (1991).
25. Li, C. *et al.* The synthesis, antileukemic activity, and crystal structures of indirubin derivatives. *Bull. Chem. Soc. Jpn* **69,** 1621–1627 (1996).
26. Wu, K. M., Zhang, M. Y., Fang, Z. & Huang, L. Potential antileukemic agents, synthesis of derivatives of indirubin, indigo and isoindigotin. *Acta Pharm. Sin.* **20,** 821–826 (1985).
27. Chang, C. N. in *Advances in Chinese Medicinal Materials Research* (eds Chang, H. M., Yeung, H. W., Tso, W., Koo, A.) 369–376 (World Scientific Pub. Co., Singapore, 1985).
28. Wan, J. H., You, Y. C., Mi, J. X. & Ying, H. G. Effect of indirubin on hematopoietic cell production. *Acta Pharmacol. Sin.* **2,** 241–244 (1981).
29. Institute of Haematology, Chinese Academy of Medical Sciences. Experimental and clinical studies of indirubin in the treatment of CML. *Chinese J. Intern. Med.* **18,** 83–88 (1979).
30. Cooperative Group of Clinical Therapy of Indirubin. Clinical studies of 314 cases of CML treated with indirubin. *Chinese J. Intern. Med.* **1,** 132–135 (1980).
31. Gan, W. J. *et al.* Studies on the mechanism of indirubin action in treatment of chronic myelocytic leukemia (CML). II. 5'-Nucleotidase in the peripheral white blood cells of CML. *Chinese J. Hematol.* **6,** 611–613 (1985).
32. Zhang, Z. N. *et al.* Treatment of chronic myelocytic leukemia (CML) by traditional Chinese medicine and Western medicine alternatively. *J. Trad. Chinese Med.* **5,** 246–248 (1985).
33. Ma, M. & Yao, B. Progress in indirubin treatment of chronic myelocytic leukaemia. *J. Trad. Chinese Med.* **3,** 245–248 (1983).
34. Jiang, S.Z. *et al.* Adverse effects of indirubin on cardiovascular system. *Chinese J. Hematol.* **7,** 30 (1986).
35. Morgan, D. Cyclin-dependent kinases: engines, clocks, and microprocessors. *Annu. Rev. Cell Dev. Biol.* **13,** 261–291 (1997).
36. Meijer, L. & Kim, S. H. Chemical inhibitors of cyclin-dependent kinases. *Methods Enzymol.* **283,** 113–128 (1997).
37. Meijer, L. *et al.* Biochemical and cellular effects of roscovitine, a potent and selective inhibitor of the cyclin-dependent kinases cdc2, cdk2 and cdk5. *Eur. J. Biochem.* **243,** 527–536 (1997).
38. Schulze-Gahmen, U. *et al.* Multiple modes of ligand recognition: crystal structures of cyclin-dependent protein kinase 2 in complex with ATP and two inhibitors, olomoucine and isopentenyladenine. *Proteins Struct. Funct. Genet.* **22,** 378–391 (1995).
39. De Azevedo, W. F. *et al.* Structural basis for specificity and potency of a flavonoid inhibitor of human CDK2, a cell cycle kinase. *Proc. Natl Acad. Sci. USA* **93,** 2735–2740 (1996).
40. De Azevedo, W. F. *et al.* Inhibition of cyclin-dependent kinases by purine analogues: crystal structure of human cdk2 complexed with roscovitine. *Eur. J. Biochem.* **243,** 518–526 (1997).
41. Gray, N. *et al.* Exploiting chemical libraries, structure, and genomics in the search for new kinase inhibitors. *Science* **281,** 533–538 (1998).
42. Lawrie, A. M. *et al.* Protein kinase inhibition by staurosporine revealed in details of the molecular interaction with CDK2. *Nature Struct. Biol.* **4,** 796–800 (1997).
43. De Bondt, H.L. *et al.* Crystal structure of cyclin-dependent kinase 2. *Nature* **363,** 595–602 (1993).
44. Russo, A., Jeffrey, P. D. & Pavletich, N. P. Structural basis of cyclin-dependent kinase activation by phosphorylation. *Nature Struct. Biol.* **3,** 696–700 (1996).
45. Knighton, D.R. *et al.* Structure of a peptide inhibitor bound to the catalytic subunit of cyclic adenosine monophosphate-dependent protein kinase. *Science* **253,** 414–420 (1991).
46. Brown, N. R. *et al.* Effects of phosphorylation of threonine 160 on CDK2 structure and activity. *J. Biol. Chem.* (in the press).
47. Otwinowski, Z. in *Oscillation Data Reduction Program* (eds Sawyer, L., Isaacs, N. & Bailey, S.) 56–62 (SERC Lab., Daresbury, Warrington, UK, 1993).
48. Collaborative Computional Project No. 4. The CCP4 suite: programs for protein crystallography. *Acta Crystallogr. D* **50,** 760–763 (1994).

ACKNOWLEDGEMENTS

We thank N. Xiuren for his help with Chinese ideogram; the fishermen of the Station Biologique de Roscoff for collecting the starfish; D. Alessi, M. Cobb, W. Harper, F. Hofmann, J. Lahti, S. Lohmann, H. Mett, D. Morgan, L. Pinna and H. Y. L. Tung for providing reagents and purified enzymes; D. Louvard, M. Mareel, M. Crepin and J.P. Moulinoux for providing cell lines; the scientists at the X-ray diffraction beamline, Elettra, Trieste; W. Burmeister for assistance during data collection on ID14-3 at the ESRF; and S. Lee, R. Bryan, K. Measures and I. Taylor for assistance. This research was supported by grants from the Association pour la Recherche sur le Cancer and the Conseil Régional de Bretagne (to L.M.), from the BBSRC, MRC and the Royal Society (to J.A.E. and M.E.M.N.) and from the German Bundesministerium für Bildung, Wissenschaft, Forschung und Technologie (to G.E.).
Correspondence and requests for materials should be addressed to L.M. or G.E.

Supplementary Information is available on Nature Cell Biology's World-Wide Web site (http://cellbio.nature.com) or as paper copy from the London editorial office of Nature Cell Biology.

